Early extensional salt tectonics controls deep-water sediment dispersal

Davide Oppo[1], Christopher A-L Jackson[2], and Vittorio Maselli[3]

[1] Sedimentary Basins Research Group, School of Geosciences, University of Louisiana at Lafayette, Lafayette 70503, LA, US

[2] Landscapes and Basins Research Group (LBRG), Department of Earth Science & Engineering, Imperial College, Prince Consort Road, London, SW7 2BP, UK

[3] Università degli Studi di Modena e Reggio Emilia, Via Università 4, 41121, Modena, Italy.

This manuscript is a preprint and is submitted for publication to a scientific journal. As a function of the peer-reviewing process, its structure and content may change. If accepted, the final version of this manuscript will be available via the 'Peer-reviewed Publication DOI' link on the right-hand side of this webpage. Please feel free to contact any of the authors; we welcome feedback.

ABSTRACT

Predicting the distribution of sedimentary facies during the early stages of deformation of salt-detached continental margins is key to constraining the location and stratigraphic architecture of hydrocarbon and CO_2 reservoirs, as well as understanding the oceanic carbon cycle. Despite its importance, we still have a relatively poor understanding of salt-sediment interactions during the early phases of extensional salt tectonics, mainly because subsequent salt-related deformation and/or deep burial of the related stratigraphic succession means the related deposits are poorly imaged in seismic reflection data and/or not penetrated by borehole data. Using 3D seismic reflection data from the northern Levant Basin offshore Lebanon, here we investigate the interplay between early extension-related salt deformation and deep-water sediment dispersal. Our results indicate that salt tectonics has two contrasting impacts: whereas slope-parallel faults favor early sediment transfer along downslope-oriented corridors to the abyssal plain, slope-normal faults and ramp-syncline basins trap land-derived sediments hampering or delaying their transport to the abyssal plain. These results help refine source-to-sink models of turbidite systems developing in young salt basins, highlighting the crucial role of extensional tectonics in controlling sediment dispersal and the development of intra-slope depocenters, and emphasizing the impact of fault strike, ramp-syncline basin evolution, and salt thinning. Our study has significant implications for predicting the location of deep-water coarse-grained sediment and the preservation of land-derived organic carbon in mature, more structurally complex salt basins.

INTRODUCTION

Determining how slope to deep-water sediment dispersal systems interact with seafloor structures is key to understanding how, how much, and where sediment is trapped along continental margins or, conversely, delivered to ocean basins. The distribution of sedimentary facies along continental margins can provide insights into how Earth's climatic and oceanographic system has changed over geological timescales, and the role played by deep-water depositional systems in sequestering carbon (Kennedy and Wagner, 2011; Mignard et al., 2017, 2017; McNeill et al., 2019; Graves et al., 2022; Liu et al., 2023). Submarine turbidity currents are crucial for transferring a significant mass of organic carbon to the deep-water system (Rabouille et al., 2019; Baker et al., 2024), and a thorough understanding of the geological processes that govern carbon dispersal, deposition, and sequestration along continental margins is essential for assessing the significance of this carbon reservoir on the global carbon cycle (Graves et al., 2022).

Predicting the distribution and stratigraphic architecture of sedimentary deep-water facies along continental margins can also guide resource exploration and utilization. For example, sandstone-dominated deep-water systems typically thin, onlap, and undergo complex lithological changes towards syn-depositional salt structures, thereby controlling the distribution, architecture, and ultimate performance of related hydrocarbon and carbon (i.e., Carbon Capture and Storage or 'CCS') reservoirs (Niemi et al., 2017; Gray et al., 2022).

Salt tectonics has a profound impact on slope structure and the overall evolution of sediment deposition along continental margins, meaning salt basins are a key archive for recording past geological change through their stratigraphic record (Pichel et al., 2018; Oppo et al., 2023). For example, numerous studies have focused on how salt-induced deformation and sediment gravity currents, such as turbidity currents and debris flows, interact with seabed structures to build deep-water channels and lobes (e.g., Loncke et al., 2006; Gee and Gawthorpe, 2006; Oluboyo et al., 2014; Howlett et al., 2021). These studies have typically focused on the distal, contraction-dominated parts of mature salt-tectonic systems (e.g., circum-Gulf of Mexico, offshore eastern Canada, circum-South Atlantic), where seafloor relief may trap or deflect sediment delivered from the basin margin, commonly resulting in fill-and-spill style depositional patterns (Galloway, 1975). In contrast, the impact of seafloor deformation in the updip, extension- and translation-dominated domains has been, to our knowledge, very rarely documented. The only notable exception is the study by Anderson et al. (2000), who show that long-term (c. 12 Myr) changes in fault-sediment interactions offshore Angola reflect gross variations in (salt-detached) fault-driven accommodation vs. sediment accumulation rate. These variations are expressed as an overall decrease in confinement, principally driven by an increase in sediment supply.

Whereas interactions between salt-induced seafloor deformation and deep-water depositional systems are relatively well-characterized in modern (i.e., at- or near-seabed) systems developed in the distal parts of salt-influenced continental margins, they are poorly constrained during the early phases of deformation and basin development. This at least partly reflects the fact that subsequent salt-tectonic deformation and, in particular, subsidence leads to the deep burial (and thus poor seismic imaging) of the related stratigraphic record. Such interactions, in addition to ramp-syncline basins (RSB), a relatively common type of salt-related depocentre that forms slightly downdip of the extensional domain (e.g., Pichel et al., 2018), are not captured in generic models illustrating salt-sediment interactions on salt-detached slopes (e.g., Oluboyo et al., 2014; Cumberpatch et al., 2021; Howlett et al., 2021). For example, beyond containing landward-dipping and -thickening wedges of slope strata (e.g., Pichel et al., 2018), there has been no detailed documentation of the types of depositional systems deposited and preserved within RSBs.

Salt in the Eastern Mediterranean Sea is relatively young (<6 Myr) and as a result, it and its relatively seismically well-imaged overburden have yet to experience intense deformation. We therefore use 3D seismic reflection data from the northern Levant Basin, eastern Mediterranean (Fig. 1), to investigate the relationship between early extension-related, salt-tectonic deformation and deep-water sediment dispersal, thereby helping refine source-to-sink models of salt-controlled depositional systems. Our results can be applied when trying to predict deep-water stratigraphy in more strongly deformed and/or deeply buried salt basins globally, where borehole data may be sparse and/or seismic reflection imaging poor.

GEOLOGICAL SETTING

The Miocene to recent stratigraphy of the Levant Basin comprises evaporites (Messinian Salt) capped by up to 2 km of predominantly deep-water clastic deposits (Haq et al., 2020; Kabir et al., 2022; Oppo et al., 2023). Messinian Salt and its overburden were moderately deformed in response to westward gravity gliding induced by post-Pleistocene tilting and uplift of the northern Levantine margin (Cartwright and Jackson, 2008). Salt-detached gliding produced domains of updip extension and downslope contraction, kinematically linked via a translational domain (Evans et al., 2021; Oppo et al., 2021).

In the extensional and translational domains, the salt and its overburden translate across several NE-trending, base-salt anticlines (Figs. 2, 3). These structures formed during the Late Miocene, prior to salt deposition, as a result of NW-SE-oriented regional convergence (Ghalayini et al., 2014; Evans et al., 2021). In the study area, these base-salt anticlines are generally asymmetrical, displaying a steep forelimb and a gently dipping backlimb (Figs. 2A, B), suggesting they represent thrust-related, fault-propagation folds (Ghalayini et al., 2014, 2018)

Translation of Messinian salt and its overburden over the base-salt anticlines lead to the formation of several salt-detached RSBs in the outer part of the extensional domain and proximal part of the translational domain (Figs. 2A, B) (Evans et al., 2021). This process created and continues to create, localized, asymmetric, synclinal depocenters immediately basinward of the base-salt anticlines. Syn-kinematic (growth) strata within the RSBs formed landward-thickening wedges that onlap landward toward the updip high (Jackson and Hudec, 2005; Pichel et al., 2018; Evans and Jackson, 2019). Critically, with ongoing translation, the at-seabed depocenter remains stationary, whereas previously RSB-hosted deposited sediments are gradually displaced basinward in the direction of salt flow (Jackson & Hudec, 2005, Pichel et al., 2018, Evans et al., 2021).

Our study area is located in the extensional and proximal translational domains (Fig. 1). In this part of the Levant Basin, the extensional domain is dominated by reactive diapirism associated with predominantly N-S-striking, basinward-dipping, and salt-detached normal faults, some of which are expressed on the present seafloor. Margin-normal (i.e., E-trending) reactive diapirs and associated salt-detached faults are also observed, in addition to the RSBs, which extend downdip into the proximal part of the translational domain (Fig. 1B) (Evans et al., 2021).

The post-Messinian deep-water stratigraphy in the North Levant Basin has, to the best of our knowledge, only been described by Maselli et al. (2021), who investigated the spatial and temporal evolution of bedforms in a single, near-seabed (i.e., Recent), deep-water lobe, which is offset by a salt-detached normal fault. They highlighted that extensional salt tectonics has had and likely continues to play a key role in controlling deep-water sedimentation and stratigraphic development.

DATA AND METHODS

We use a 3D time-migrated seismic reflection dataset that is near-zero phase at the seafloor reflection and is displayed here with SEG negative polarity, i.e., downward increase and decrease in acoustic impedance are represented by a trough (blue in our seismic displays) and peak (red in our seismic displays) reflection, respectively (Brown, 2001). The dominant frequency in the post-salt overburden, extracted directly from the seismic dataset, is 50 Hz, with an average P-wave velocity of 2,000 m/s indicated by proprietary processing reports. Based on these data, the estimated vertical resolution for the post-salt overburden is ~10 m. The horizontal resolution is ~25 m, approximated as a quarter of the dominant wavelength (Lebedeva-Ivanova et al., 2018). As described below, these data are of sufficient quality to image the main salt-tectonic structures and the key depositional elements in the overburden.

The lack of well data offshore Lebanon prevents a precise calibration of the lithology and age of the overburden. We therefore use seismic facies analysis and the root mean square (RMS) attribute extractions to infer depositional system types and sediment grain size. More specifically, following Maselli et al. (2021) and other studies of deep-water seismic geomorphology (e.g., Prather et al., 1998), we interpret high RMS values as representing coarser, likely sand-rich sediment. The only absolute age is provided by the 1.8 Ma reflection, correlated from Oppo et al. (2021). However, the excellent seismic data quality means we can confidently establish a robust seismic-stratigraphic framework to define the relative if not absolute age of various depositional elements.

RESULTS

In the south of the study area, a U-shaped incision at the seafloor extends from the shelf to the slope and is filled with generally high-amplitude, relatively continuous reflections (Fig. 1C). This incision is interpreted as a channel that delivers sediment to the abyssal plain (Channel A). Channel A extends from the base-of-slope to the abyssal plain, crossing the extensional domain, where it is confined laterally by margin-normal and -oblique faults that displace seismic reflections up to the seafloor (Fig.1). In the easternmost, most proximal part of the survey, Channel A is underlain by stacked paleochannels that progressively migrate laterally (Figs. 4A, B). The oldest paleochannels developed at ca. 1.8 Ma, indicating this is a relatively long-lived system. Less than 5 km basinward, the stacked paleochannels disappear from the stratigraphy, and only the seabed expression of Channel A is present (Figs. 4C, D). Stacked paleochannels are also absent throughout the extensional domain, where the channel stratigraphy is mainly formed by high-amplitude, variable continuity seismic reflections, which are locally preserved within margin-normal grabens (Figs. 5A-D).

Upon reaching the abyssal plain, Channel A encounters an RSB that contains sheet-like, high-amplitude reflections at its base (Figs. 5E, 6). This high-amplitude unit shows an overall fan-shaped geometry, extending up to c. 7 km laterally from the modern Channel A. To the SW, the high-amplitude reflections downlap onto the basal units of the RSB, whereas to the NE they interfinger with the surrounding, lower-amplitude stratigraphy. At the top, the unit of high-amplitude reflections is variably incised by stacked, U-shaped channels that are filled with high-amplitude reflections (Fig. 5E). We interpret the high-amplitude unit at the base of the RSB as a package of stacked, deep-sea lobes, based on their acoustic and geometric resemblance to similar features documented elsewhere (Prather et al., 1998, p. e.g.,; Prather, 2003; Maselli et al., 2021). Differently from the stacked channels, within the lobes, the main channel, Channel A, is defined by relatively low-amplitude reflections, suggesting it is finer-grained than its encasing unit (Figs.5E, 7). Further basinward, the channel encounters a second RSB (Figs. 5G, 6), where at least two stacked lobes, larger than the ones in the updip RSB, occur. Like those in the updip RSB, these lobes are defined by high-amplitude reflections and are incised by Channel A, which again is filled by low-amplitude reflections (Figs. 5G, 7). Above the lobes, stacked channels transition to laterally continuous, high-amplitude reflections, which are visible only in the near-seafloor interval, and which are not incised by channels (Fig. 5G). We interpret these continuous reflections as a shallower, more recent lobe.

Once it exits the second RSB, the channel becomes less confined (Fig. 7), with the underlying stratigraphy being defined by well-developed, reflective, presumably sandy paleochannels (Figs. 2, 7). The stratigraphic relationship between the 1.8 Ma reflection and lobes in the downdip RSB/abyssal plain suggests that the onset of sandy deposition was broadly coincident with the initiation of the oldest paleo-channel observed in the most proximal part of the survey (Fig. 4).

A second channel (Channel B) is present c. 8.6 km north of Channel A. Channel B shares many similarities with Channel A, i.e., it extends from the base-of-slope to the abyssal plain, crossing the salt-detached extensional domain (Fig. 1), and proximal to the base-of-slope is underlain by stacked paleochannels that developed after ca. 1.8 Ma (Fig. 4A), but which are absent from the stratigraphy immediately basinward of the first margin-parallel, salt-related graben, G1 (Figs. 1B, 4C). Unlike Channel A, however, Channel B is not laterally confined by faults at the base-of-slope, where it instead trends slope-parallel. Further downslope, in the central, more heavily faulted area, the channel abruptly turns 90° northward upon entering a margin-parallel graben (G2 in Fig. 1B), and then 90° westward, where it exits G2 before passing onto the abyssal plain and becoming relatively sinuous (Fig. 1). Seismic sections across this tract of the channel show that it has an erosional base and is underfilled (Fig. 8C). On the abyssal plain, downslope of the extensional domain, Channel B has a moderately erosional base and is bounded by small levees (Fig. 8E), before passing downslope into at-seabed (i.e., Recent) lobes (Figs. 1C, 8G).

INTERPRETATION

Our data suggest that early salt deformation in the extensional and proximal translational domains of a salt-detached slope controlled the sequestration and routing of deep-water sediment and the ultimate stratigraphic evolution of related channels and lobes. We interpret two main styles of salt-sediment interaction: (1) early and sustained delivery of coarse-grained sediment to the abyssal plain (as exemplified by Channel A), and (2) initial sequestration of sediment at the base-of-slope, with subsequent bypass of the extensional domain (as exemplified by Channel B).

Channel A – Early delivery to the abyssal plain

The stratigraphic relationship between the paleochannels, the downslope paleo-lobes, and the 1.8 Ma reflection, indicates that coarse-grained sediment supply to the abyssal plain was established in the Early Pleistocene. Time-equivalent paleochannels at the base-of-slope and on the abyssal plain indicate that Channel A connected these two areas despite the lack of obvious paleochannel-related incisions across the extensional domain. We interpret that the apparent absence of incision reflects the combined effects of structural confinement by margin-normal and -oblique faults and related grabens, and the elevated sediment supply, which together caused channel filling, inhibited erosion, and aided basinward propagation of the channel (Fig. 5). As a result, coarse sediment was delivered through the extensional domain directly to lobes on the abyssal plain, in the proximal part of the translational domain (Figs. 2, 6).

Notably, however, upon reaching the abyssal plain, salt-detached translation still influenced sedimentation patterns, with RSBs at least temporarily providing accommodation for the local preservation of lobes. More specifically, we infer that the deposition of a sandy lobe in the updip RSB was followed by channel incision and coarse sediment bypass to the downdip RSB, where a stacked set of sandy lobes were deposited before the channel was filled by finer-grained material. These lobes were then incised by their feeder channel, which propagated basinward, delivering sediments to the most distal part of the abyssal plain. We suggest that the shallowest lobe within the downdip RSB (Fig. 6G) formed during a period of reduced incision, possibly due to a reduced gradient and/or supply during higher sea level. The deposition of coarse-grained sediment within the RSB, and its subsequent incision by a younger channel that was ultimately filled by finer-grained material, records the progressive basinward migration of the slope depocenter and bypassing coarse sediment to the distal abyssal plain. These depositional patterns are comparable to those captured in traditional deep-water fill-and-spill models, where the relationship between accommodation and sediment accumulation rates controls depocenter filling vs. bypass (e.g., Prather, 2003). In this example, salt-detached translation, rather than minibasin subsidence (e.g., Prather et al., 1998) or contractional growth folding (e.g., Smith, 2004), caused the local development of intra-slope accommodation. The rate at which salt-detached translation and, by extension, accommodation development occurs within an RSB are mainly controlled by salt translation, driven by tectonic tilting of the basin margin, salt differential loading by the overburden, and flow disequilibrium across the underlying anticlines (Allen et al., 2016; Evans et al., 2021; Granado et al., 2023). Flow disequilibrium results in salt flow pulses (Evans et al., 2021), leading to cyclical variations in local translation rates, impacting how, where, and how much sediment is deposited or bypassed in these highly dynamic systems. In particular, salt thickness above base-salt anticlines controls the rate of basinward salt flow, with faster or slower translation rates resulting in increases or decreases of accommodation, respectively (Wagner and Jackson, 2011). In the latter case, when sediment supply is relatively high, the overall aggradation will also be high, giving rise to a fill-and-spill system. Given that thick, stacked lobe-dominated successions are not preserved in the documented RSBs, and that an overall fill-and-spill pattern is recorded, we suggest that RSB (horizontal) translation and (vertical) subsidence rate were low relative to sediment supply, thus favoring the delivery of coarse sediment to the distal basin in a relatively short period (<1.8 Myr) after channel establishment on the upper slope.

Channel B – Early sequestration at the base-of-slope

Based on their stratigraphic relationship to the 1.8 Ma reflection, we infer the paleochannels associated with Channel B also initiated in the Early Pleistocene, at broadly the same time as Channel A. However, the lack of paleochannels, paleo-lobes, and other stratigraphic evidence of coarse-grained sediment delivery to, or at least preservation within, the extension and proximal translational domain, indicates that Channel B did not reach the deeper basin until relatively recently. This suggests that the most proximal margin-parallel, intra-slope graben (G1) efficiently trapped coarse-grained sediment, stopping it from reaching the base-of-slope and abyssal plain (Fig. 8A). Like Channel A, the depositional patterns described here are comparable to those captured in deep-water fill-and-spill models. Critically, however, at least during the earliest phase of development of Channel B, we only observe the 'fill' phase.

Over time, Channel B migrated southwards, beyond the southern limit of G1 (Fig. 1, 4C). This, possibly coupled with slower subsidence and rate of accommodation development due to progressive salt thinning, allowed the channel to ultimately escape from G1 and extend basinward. However, the channel was eventually (and continues to be) partly confined by the next downslope graben (G2). Within this new depocentre, the strongly erosional character of the channel (Fig. 8C) suggests that confinement favored (and perhaps still favors) sediment bypass through the entire upper course of the channel.

CONCLUSION AND IMPLICATIONS

The large-scale tectono-stratigraphic architecture and development of salt-detached RSBs is described from offshore Nova Scotia (e.g., Saint-Ange et al., 2017), Morocco (e.g., Uranga et al., 2022), and Brazil (e.g., Pichel et al., 2018). However, the detailed stratigraphic evolution of the deep-water systems they contain has yet to be thoroughly investigated. Our study shows that extensional tectonics during the early stages of salt-detached extension and translation profoundly controls sediment routing to the abyssal plain. More specifically, slope-parallel faults focus turbidity currents, favoring early sediment transfer through the extensional domain, whereas slope-normal faults and RSBs generate considerable accommodation, thus favoring trapping and deflection of deep-water channels and the accumulation of coarse sediment in the extensional and (proximal) translational domains . In the latter case, those structures reduce the seafloor gradient and cause turbidity currents to decelerate, depositing the coarse-grained fractions and allowing the development of a lobe (Maselli et al., 2021). It is possible that the finer-grained fraction of these flows continue distally and in our case, are reworked into the low-amplitude sediment waves observed on the abyssal plain (Fig. 1A). Eventually, lateral channel migration and/or the cessation of accommodation generation due to progressive salt thinning allow the channel to transfer coarser-grained sediment toward and onto the abyssal plain. Therefore, the interplay between 1) the rate of the seaward flow of salt, 2) RSB translation rate and accommodation development, and 3) sediment supply and accumulation in RSBs dictates the evolution of coarse-grained sediment depocenters and, ultimately, delivery of material to ocean basins.

The role of slope-parallel grabens and RSBs in trapping sediment within proximal, base-of-slope areas could also have significant implications for the complex dynamics of organic carbon transport to the abyssal plain. Large volumes of carbon originating from land or shelf regions are transferred to the deep sea via turbidity currents (Galy et al., 2007; Pope et al., 2022; Talling et al., 2024; Baker et al., 2024), and may be temporarily or permanently stored in these grabens and within intra-RSB lobes, facilitated by high subsidence and sedimentation rates that rapidly isolate the carbon from the oxidizing conditions near the seafloor. Over time, incision of the intra-RSB lobes by turbidity currents (Baker et al., 2024) may result in the re-suspension and oxidation of previously buried carbon.

Our results also provide insights into early-stage, deep-water distribution of sedimentary facies in salt basins that are now strongly deformed in response to ongoing tectonics, with important implications for the exploration for and development of hydrocarbon or CO_2 reservoirs. For example, we demonstrate that turbidite sandstone-dominated, deep-water lobes and channels, initially deposited at modest burial depths near the base-of-slope, can be translated over considerable distances, potentially exceeding 10 km, whilst becoming progressively more deeply buried in the sedimentary column. This results in reservoirs extending further basinward than traditionally predicted by deep-water depositional models, challenging existing exploration models and indicating that potential reservoir targets might be located in areas previously considered unprospective. Fluctuations in sediment accumulation rates and salt-induced accommodation, and the related processes of fill, spill, bypass, and channel incision, for example where a sandstone-rich lobe is incised by the mudstone-filled Channel A, may also result in significant heterogeneity and compartmentalization within the reservoirs (e.g., Mayall et al., 2006). For example, this stratigraphic complexity could influence fluid injectivity, storage capacity, flow, and the overall long-term containment capacity of CO_2 storage reservoirs.

In summary, our study highlights that fault strike relative to sediment input direction, RSB development and evolution, and the temporal relationship between sediment input and salt thinning all need to be captured in tectonostratigraphic models for salt basins, given these dictate if and where land-derived material is delivered to the deep ocean, as well as the distribution and architecture of subsurface reservoirs.

ACKNOWLEDGMENTS

We acknowledge W. Chbat and the Lebanese Petroleum Administration for providing data and Schlumberger for granting Petrel© academic licenses. We thank the Science Editor, Dr. Ducea, the reviewer, Dr. Granado, and one anonymous Associate Editor and one anonymous reviewer for their thorough revision and helpful comments.

REFERENCES CITED

Allen, H., Jackson, C.A.-L., and Fraser, A.J., 2016, Gravity-driven deformation of a youthful saline giant: the interplay between gliding and spreading in the Messinian basins of the Eastern Mediterranean: Petroleum Geoscience, v. 22, p. 340–356, doi:10.1144/petgeo2016-034.

Anderson, J.E., Cartwright, J., Drysdall, S.J., and Vivian, N., 2000, Controls on turbidite sand deposition during gravity-driven extension of a passive margin: examples from Miocene sediments in Block 4, Angola: Marine and Petroleum Geology, v. 17, p. 1165–1203, doi:10.1016/S0264-8172(00)00059-3.

Baker, M.L. et al., 2024, Globally significant mass of terrestrial organic carbon efficiently transported by canyon-flushing turbidity currents: Geology, v. 52, p. 631–636, doi:10.1130/G51976.1.

Brown, A.R., 2001, Color in seismic display: The Leading Edge, v. 20, p. 549–549, doi:10.1190/1.1438992.

Cartwright, J.A., and Jackson, M.P.A., 2008, Initiation of gravitational collapse of an evaporite basin margin: The Messinian saline giant, Levant Basin, eastern Mediterranean: Geological Society of America Bulletin, v. 120, p. 399–413, doi:10.1130/B26081X.1.

Cumberpatch, Z.A., Kane, I.A., Soutter, E.L., Hodgson, D.M., Jackson, C.A.-L., Kilhams, B.A., and Poprawski, Y., 2021, Interactions between deep-water gravity flows and active salt tectonics: Journal of Sedimentary Research, v. 91, p. 34–65, doi:10.2110/jsr.2020.047.

Evans, S.L., and Jackson, C.A. -L., 2019, Base-salt relief controls salt-related deformation in the Outer Kwanza Basin, offshore Angola: Basin Research, p. bre.12390, doi:10.1111/bre.12390.

Evans, S.L., Jackson, C.A.-L., and Oppo, D., 2021, Taking the Pulse of Salt-Detached Gravity Gliding in the Eastern Mediterranean: Tectonics, v. 40, p. e2020TC006476, doi:https://doi.org/10.1029/2020TC006476.

Galloway, W.E., 1975, Process Framework for Describing the Morphologic and Stratigraphic Evolution of Deltaic Depositional Systems: Deltas: Models for Exploration, p. 87–98.

Galy, V., France-Lanord, C., Beyssac, O., Faure, P., Kudrass, H., and Palhol, F., 2007, Efficient organic carbon burial in the Bengal fan sustained by the Himalayan erosional system: Nature, v. 450, p. 407–410, doi:10.1038/nature06273.

Gee, M.J.R., and Gawthorpe, R.L., 2006, Submarine channels controlled by salt tectonics: Examples from 3D seismic data offshore Angola: Marine and Petroleum Geology, v. 23, p. 443–458, doi:10.1016/j.marpetgeo.2006.01.002.

Ghalayini, R., Daniel, J.-M., Homberg, C., Nader, F.H., and Comstock, J.E., 2014, Impact of Cenozoic strike-slip tectonics on the evolution of the northern Levant Basin (offshore Lebanon): Cenozoic tectonics of the Levant basin: Tectonics, v. 33, p. 2121–2142, doi:10.1002/2014TC003574.

Ghalayini, R., Nader, F.H., Bou Daher, S., Hawie, N., and Chbat, W.E., 2018, PETROLEUM SYSTEMS OF LEBANON: AN UPDATE AND REVIEW: Journal of Petroleum Geology, v. 41, p. 189–214, doi:10.1111/jpg.12700.

Granado, P., Santolaria, P., and Muñoz, J.A., 2023, Interplay of downbuilding and gliding in salt-bearing rifted margins: Insights from analogue modeling and natural case studies: AAPG Bulletin, v. 107, p. 2091–2118, doi:10.1306/08072221203.

Graves, C.A. et al., 2022, Sedimentary carbon on the continental shelf: Emerging capabilities and research priorities for Blue Carbon: Frontiers in Marine Science, v. 9, doi:10.3389/fmars.2022.926215.

Gray, E., Hartley, A., and Howell, J., 2022, The influence of stratigraphy and facies distribution on reservoir quality and production performance in the Triassic Skagerrak Formation of the UK and Norwegian Central North Sea: Geological Society, London, Special Publications, v. 494, p. 379–409, doi:10.1144/SP494-2019-68.

Haq, B., Gorini, C., Baur, J., Moneron, J., and Rubino, J.-L., 2020, Deep Mediterranean's Messinian evaporite giant: How much salt? Global and Planetary Change, v. 184, p. 103052, doi:10.1016/j.gloplacha.2019.103052.

Howlett, D.M., Gawthorpe, R.L., Ge, Z., Rotevatn, A., and Jackson, C.A.-L., 2021, Turbidites, topography and tectonics: Evolution of submarine channel-lobe systems in the salt-influenced Kwanza Basin, offshore Angola: Basin Research, v. 33, p. 1076–1110, doi:10.1111/bre.12506.

Jackson, M.P.A., and Hudec, M.R., 2005, Stratigraphic record of translation down ramps in a passive-margin salt detachment: Journal of Structural Geology, v. 27, p. 889–911, doi:10.1016/j.jsg.2005.01.010.

Kabir, S.M.M., Iacopini, D., Hartley, A., Maselli, V., and Oppo, D., 2022, Seismic characterization and depositional significance of the Nahr Menashe deposits: Implications for the terminal phases of the Messinian salinity crisis in the north-east Levant Basin, offshore Lebanon: Basin Research, v. 00, p. 1–26, doi:10.1111/bre.12697.

Kennedy, M.J., and Wagner, T., 2011, Clay mineral continental amplifier for marine carbon sequestration in a greenhouse ocean: Proceedings of the National Academy of Sciences, v. 108, p. 9776–9781, doi:10.1073/pnas.1018670108.

Lebedeva-Ivanova, N., Polteau, S., Bellwald, B., Planke, S., Berndt, C., and Henriksen Stokke, H., 2018, Toward one-meter resolution in 3D seismic: The Leading Edge, v. 37, p. 794–864, doi:https://doi.org/10.1190/tle37110818.1.

Liu, X., Fan, D., Xu, F., and Liu, J.P., 2023, Editorial: Sedimentation on the continental margins: From modern processes to deep-time records: Frontiers in Earth Science, v. 10, doi:10.3389/feart.2022.1048801.

Loncke, L., Gaullier, V., Mascle, J., Vendeville, B., and Camera, L., 2006, The Nile deep-sea fan: An example of interacting sedimentation, salt tectonics, and inherited subsalt paleotopographic features: Marine and Petroleum Geology, v. 23, p. 297–315, doi:10.1016/j.marpetgeo.2006.01.001.

Maselli, V., Micallef, A., Normandeau, A., Oppo, D., Iacopini, D., Green, A., and Ge, Z., 2021, Active faulting controls bedform development on a deep-water fan: Geology, v. 49, p. 1495–1500, doi:10.1130/G49206.1.

McNeill, L.C. et al., 2019, High-resolution record reveals climate-driven environmental and sedimentary changes in an active rift: Scientific Reports, v. 9, p. 3116, doi:10.1038/s41598-019-40022-w.

Mignard, S.L.-A., Mulder, T., Martinez, P., Charlier, K., Rossignol, L., and Garlan, T., 2017, Deep-sea terrigenous organic carbon transfer and accumulation: Impact of sea-level variations and sedimentation processes off the Ogooue River (Gabon): Marine and Petroleum Geology, v. 85, p. 35–53, doi:10.1016/j.marpetgeo.2017.04.009.

Mayall, M., Jones, E., & Casey, M. (2006). Turbidite channel reservoirs—Key elements in facies prediction and effective development. Marine and Petroleum Geology, 23(8), 821–841. https://doi.org/10.1016/j.marpetgeo.2006.08.001

Niemi, A., Bear, J., and Bensabat, J. (Eds.), 2017, Geological Storage of CO2 in Deep Saline Formations: Springer Dordrecht, 554 p., https://link.springer.com/book/10.1007/978-94-024-0996-3 (accessed April 2024).

Oluboyo, A.P., Gawthorpe, R.L., Bakke, K., and Hadler-Jacobsen, F., 2014, Salt tectonic controls on deep-water turbidite depositional systems: Miocene, southwestern Lower Congo Basin, offshore Angola: Basin Research, v. 26, p. 597–620, doi:10.1111/bre.12051.

Oppo, D., Evans, S., Iacopini, D., Kabir, S.M., Maselli, V., and Jackson, C.A.-L., 2021, Leaky salt: pipe trails record the history of cross-evaporite fluid escape in the northern Levant Basin, Eastern Mediterranean: Basin Research, v. 33, p. 1798–1819, doi:https://doi.org/10.1111/bre.12536.

Oppo, D., Jackson, C.A.-L., Gorini, C., Iacopini, D., Evans, S., and Maselli, V., 2023, Mass wasting records the first stages of the Messinian Salinity Crisis in the eastern Mediterranean: Geology, v. 51, p. 637–641, doi:10.1130/G51146.1.

Pichel, L.M., Peel, F., Jackson, C.A.-L., and Huuse, M., 2018, Geometry and kinematics of salt-detached ramp syncline basins: Journal of Structural Geology, v. 115, p. 208–230, doi:10.1016/j.jsg.2018.07.016.

Pope, E.L. et al., 2022, Carbon and sediment fluxes inhibited in the submarine Congo Canyon by landslide-damming: Nature Geoscience, v. 15, p. 845–853, doi:10.1038/s41561-022-01017-x.

Prather, B.E., 2003, Controls on reservoir distribution, architecture and stratigraphic trapping in slope settings: Marine and Petroleum Geology, v. 20, p. 529–545, doi:10.1016/j.marpetgeo.2003.03.009.

Prather, B.E., Booth, J.R., Steffens, G.S., and Craig, P.A., 1998, Classification, Lithologic Calibration, and Stratigraphic Succession of Seismic Facies of Intraslope Basins, Deep-Water Gulf of Mexico1: AAPG Bulletin, v. 82, p. 701–728, doi:10.1306/1D9BC5D9-172D-11D7-8645000102C1865D.

Rabouille, C. et al., 2019, Carbon and silica megasink in deep-sea sediments of the Congo terminal lobes: Quaternary Science Reviews, v. 222, p. 105854, doi:10.1016/j.quascirev.2019.07.036.

Saint-Ange, F., Savva, D., Colletta, B., Marfisi, E., Cuilhé, L., MacDonald, A., and Luheshi, M., 2017, Salt – sediment interaction in Sable Sub-basin, Nova Scotia (Canada).

Smith, R., 2004, Silled sub-basins to connected tortuous corridors: sediment distribution systems on topographically complex sub-aqueous slopes, *in* Lomas, S.A. and Joseph, P. eds., Confined Turbidite Systems, Geological Society of London, v. 222, p. 0, doi:10.1144/GSL.SP.2004.222.01.03.

Talling, P.J., Hage, S., Baker, M.L., Bianchi, T.S., Hilton, R.G., and Maier, K.L., 2024, The Global Turbidity Current Pump and Its Implications for Organic Carbon Cycling: Annual Review of Marine Science, v. 16, p. 105–133, doi:10.1146/annurev-marine-032223-103626.

Uranga, R.M., Ferrer, O., Zamora, G., Muñoz, J.A., and Rowan, M.G., 2022, Salt tectonics of the offshore Tarfaya Basin, Moroccan Atlantic margin: Marine and Petroleum Geology, v. 138, p. 105521, doi:10.1016/j.marpetgeo.2021.105521.

FIGURE CAPTIONS

Figure 1. (A) and (C) show the bathymetry of the study area using depth in seconds and amplitude RMS seismic attribute, respectively. (B) Structural map showing the two channels (red), normal faults (black), and salt diapirs (pink). (C) The red/yellow color represents higher concentrations of coarse-grained sediment. RMS: Root Mean Square.

Figure 2. Dip seismic sections showing the overall margin setting (location in Fig. 1C). (A) and (B) are c. along Channel A, and (C) and (D) are along Channel B. Note the deep-sea lobes and the unconfined channels/fan deposits. Red faults are late to post-Messinian and are related to salt gliding toward the basin. Pink shading: Messinian Salt. RSB: Ramp syncline basin. Blue horizon: 1.8 Ma age marker marker from Oppo et al., 2021.

Figure 3. Maps of the Messinian Salt across the investigated area. The position of the modern channels are projected in white. (A) Base Salt map with indicated the main base-salt anticlines described in text. (B) Top Salt map with indicated the projection of the main salt-related normal faults rooted in the top salt units. The two RSB paleo-depocenters where the deep-sea lobes described in the text occur are indicated. (C) Salt thickness map. Note the reduced salt thickness above the base-salt anticlines causing the two RSBs in Figure 2.

Figure 4. Seismic cross-sections parallel to the margin (location in Fig. 1C) showing the channels evolution close to the base-of-slope. (A, B): Proximal seismic cross-section showing stacked channels underneath both Channel A and Channel B. Note the progressive lateral migration of the channels to the southwest. (C, D) Parallel seismic cross-section basinward to the first margin-parallel graben, G1, showing the absence of stacked paleochannels and only a relatively recent, modern channel incising the seafloor. Faults are red, Messinian Salt is pink, and sand-rich channels and lobes deposit in yellow.

Figure 5. Seismic cross-sections showing the lack of a well-developed Channel A incision within margin-perpendicular grabens (A) and half-grabens (B) across the extensional domain. (E-G) Well-developed paleochannels and deep-sea lobes are associated with Channel A

within the first (E) and the second (G) RSB (Fig. 1 for location). Faults are red, Messinian Salt is pink, and sand-rich channels and lobes deposit in yellow.

Figure 6. Seismic cross-section showing the details of the two RSBs hosting the deep-sea lobes in Channel A. Note that the channel deposits are cut circa parallel to the basinward channel development (location of the seismic section in Fig. 1), Faults are red, Messinian Salt is pink, and sand-rich channels and lobes deposit in yellow.

Figure 7. RMS amplitude calculated on the 1.8 Ma horizon showing the two deep-sea lobes formed by the deposition of coarse-grained sediment within two consecutive RSBs. A complex of unconfined channel/fan deposits is visible in the basinward portion of the data (see also Fig. 2A). Note the low amplitude of Channel A when incising the distal lobe. The dashed lines delimit the RSB paleo-depocenters.

Figure 8. Seismic cross-sections showing the basinward development of Channel B. (A, B) Section along the graben G1 showing discontinuous, moderate amplitude reflections formed by the sediments of Channel B captured by the graben. (C, D) Section parallel to the margin showing the erosional character of Channel B within graben G2. Black arrows mark strata truncation. Flow within the channel is northeastwards. (E, F) Detail of the seafloor incision and associated levees in the proximal translational domain. (G, H) Distal deep-sea lobe associated with Channel B. . Messinian Salt is pink, and sand-rich channels and lobe deposits are yellow.

20 km
N
Europe
Study area
Africa
Basiward limit of the extensional domain
Channel B
Channel A
Base-of-slope
Depth (sec)
0
-2.5
34º00'N
33º48'N
35º00'E
35º20'E
A
Salt diapirs
Basiward limit of the extensional domain
Channel B
G2
G1
Channel A
Deep-sea lobes
Margin-normal grabens
Base-of-slope
B
Fig. 8E
Fig. 8A
Fig. 2C
Fig. 8G
Fig. 4A
Fig. 7
Fig. 8C
Fig. 2A
Fig. 5A
Fig. 4C
Fig. 5B
Fig. 5E
Fig. 5F
RMS
75k
0
C

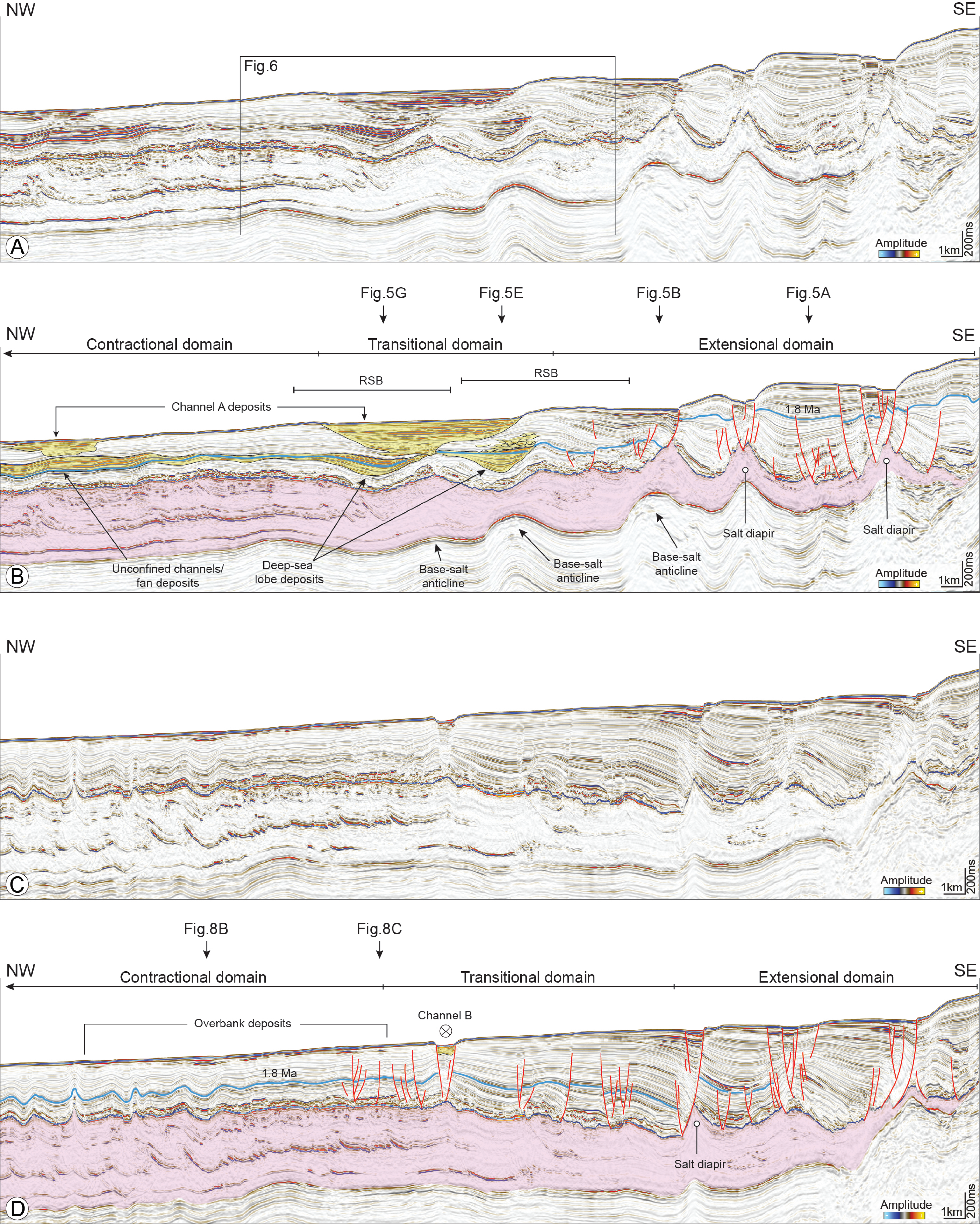

NW
SE
Fig.6
A
Amplitude
1km
200ms
Fig.5G
Fig.5E
Fig.5B
Fig.5A
NW
Contractional domain
Transitional domain
Extensional domain
SE
RSB
RSB
Channel A deposits
1.8 Ma
Salt diapir
Salt diapir
Unconfined channels/ fan deposits
Deep-sea lobe deposits
Base-salt anticline
Base-salt anticline
Base-salt anticline
B
Amplitude
1km
200ms
NW
SE
C
Amplitude
1km
200ms
Fig.8B
Fig.8C
NW
Contractional domain
Transitional domain
Extensional domain
SE
Channel B
Overbank deposits
1.8 Ma
Salt diapir
D
Amplitude
1km
200ms

20 km
N
Projection of the modern channel
Base-salt anticlines
-2.4
Depth (sec)
-3.7
A
Base Salt
RSB paleo-depocenters
-2.4
Depth (sec)
-3.2
B
Top Salt
Thinning over base-salt anticlines
0.8
Thickn (sec)
0
C
Salt Thickness

SW
NE
A
250ms
1km
Amplitude
-
+
SW
Channel A
Channel B
NE
1.8 Ma
B
250ms
1km
Amplitude
-
+
SW
NE
C
250ms
1km
Amplitude
-
+
SW
Channel A
Channel B
NE
D
250ms
1km
Amplitude
-
+

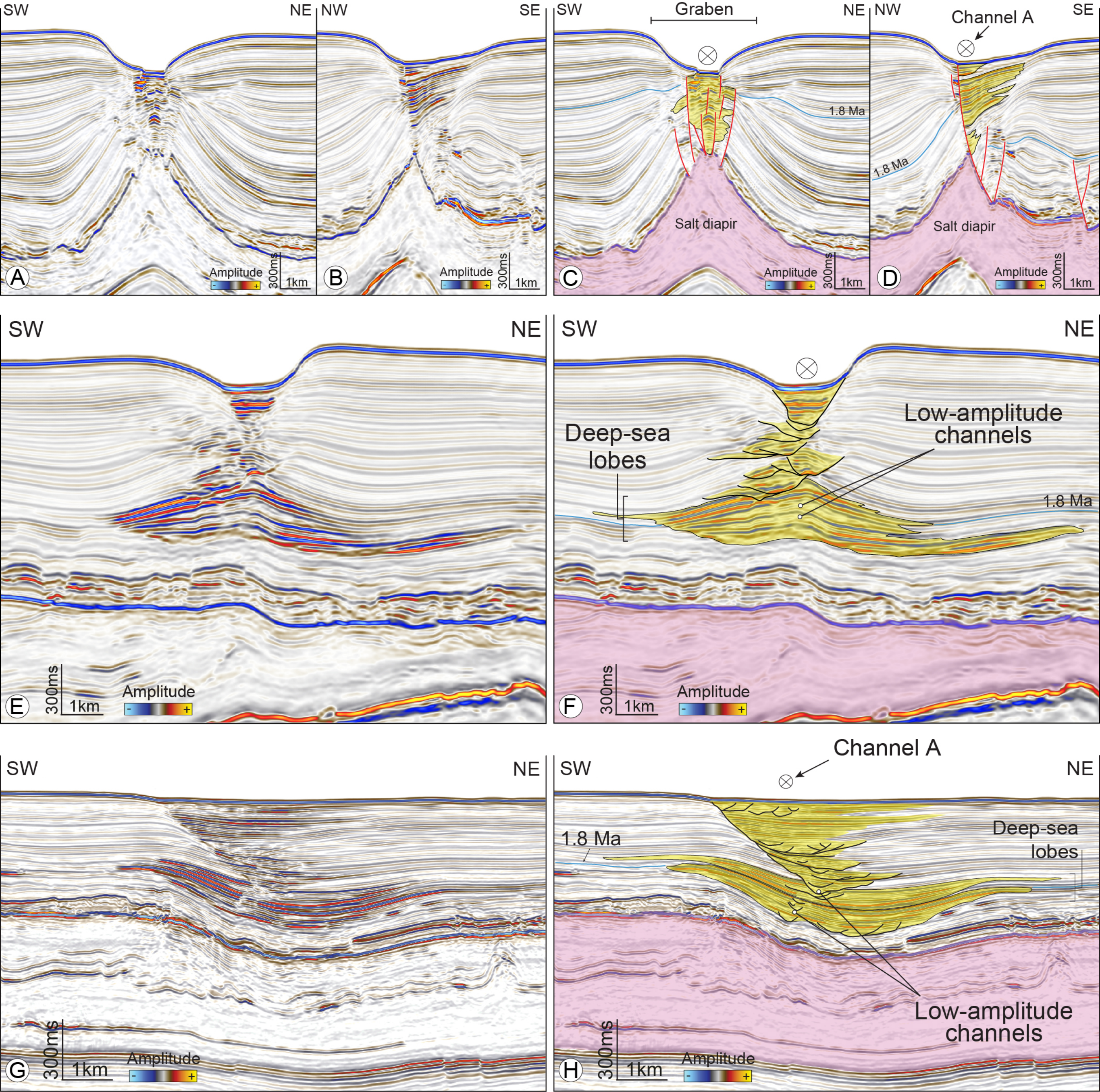

SW
NE
NW
SE
Graben
Channel A
1.8 Ma
Salt diapir
Amplitude
300ms
1km
A
B
C
D
Deep-sea lobes
Low-amplitude channels
E
F
G
H

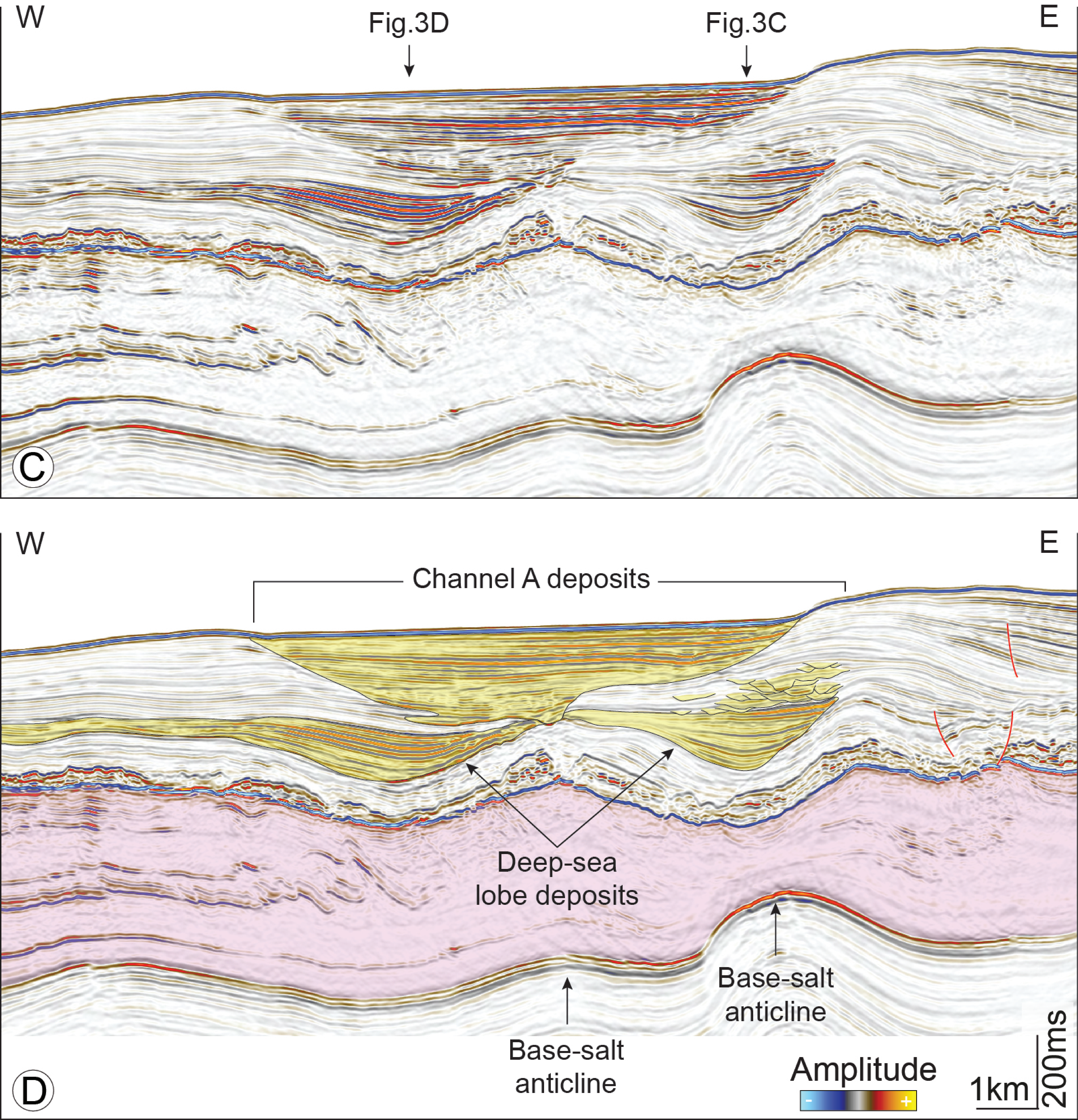
W
Fig.3D
Fig.3C
E
C
W
E
Channel A deposits
Deep-sea
lobe deposits
Base-salt
anticline
Base-salt
anticline
D
Amplitude
-
+
1km
200ms

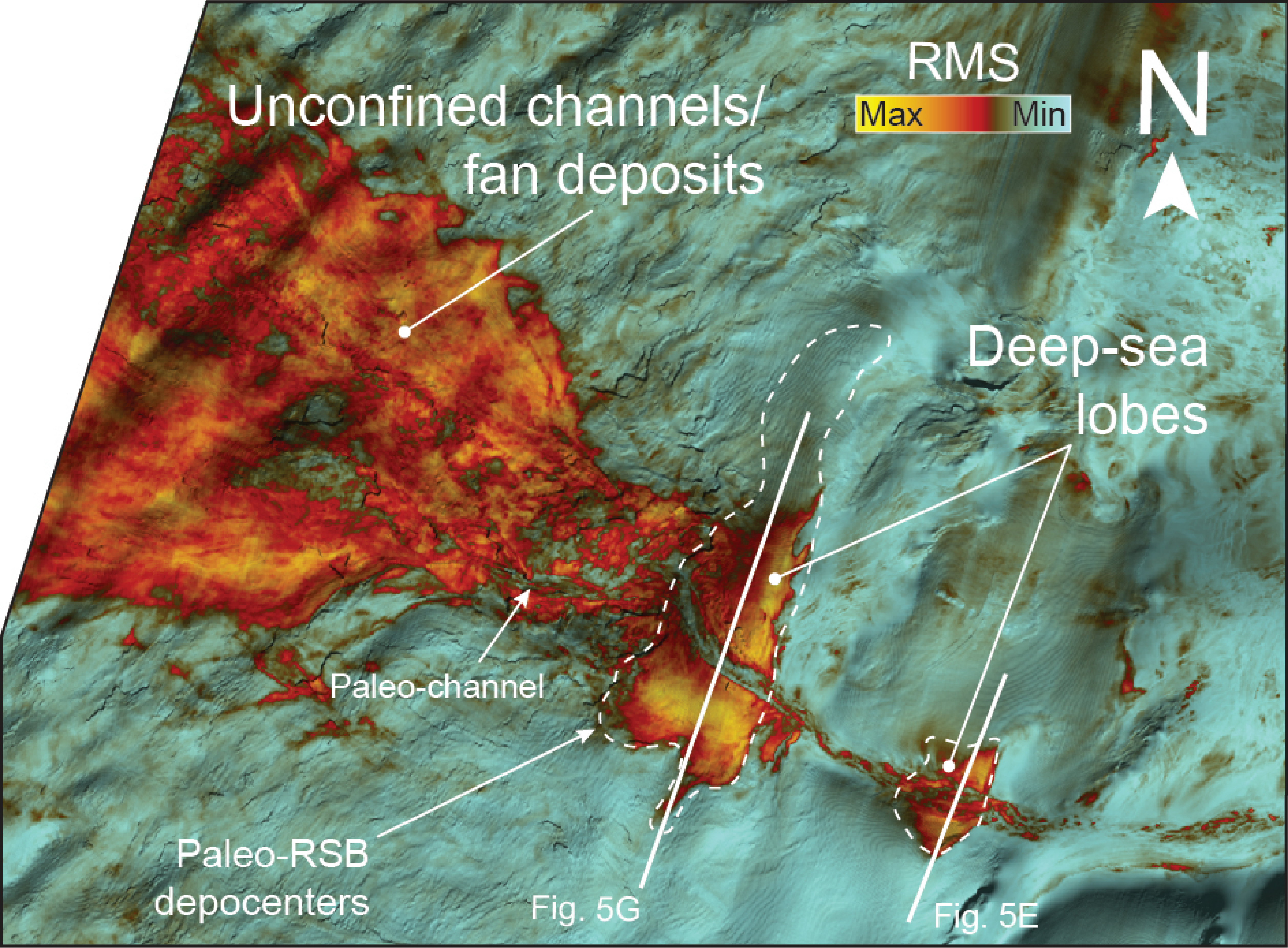

RMS
Max
Min
N
Unconfined channels/
fan deposits
Deep-sea
lobes
Paleo-channel
Paleo-RSB
depocenters
Fig. 5G
Fig. 5E

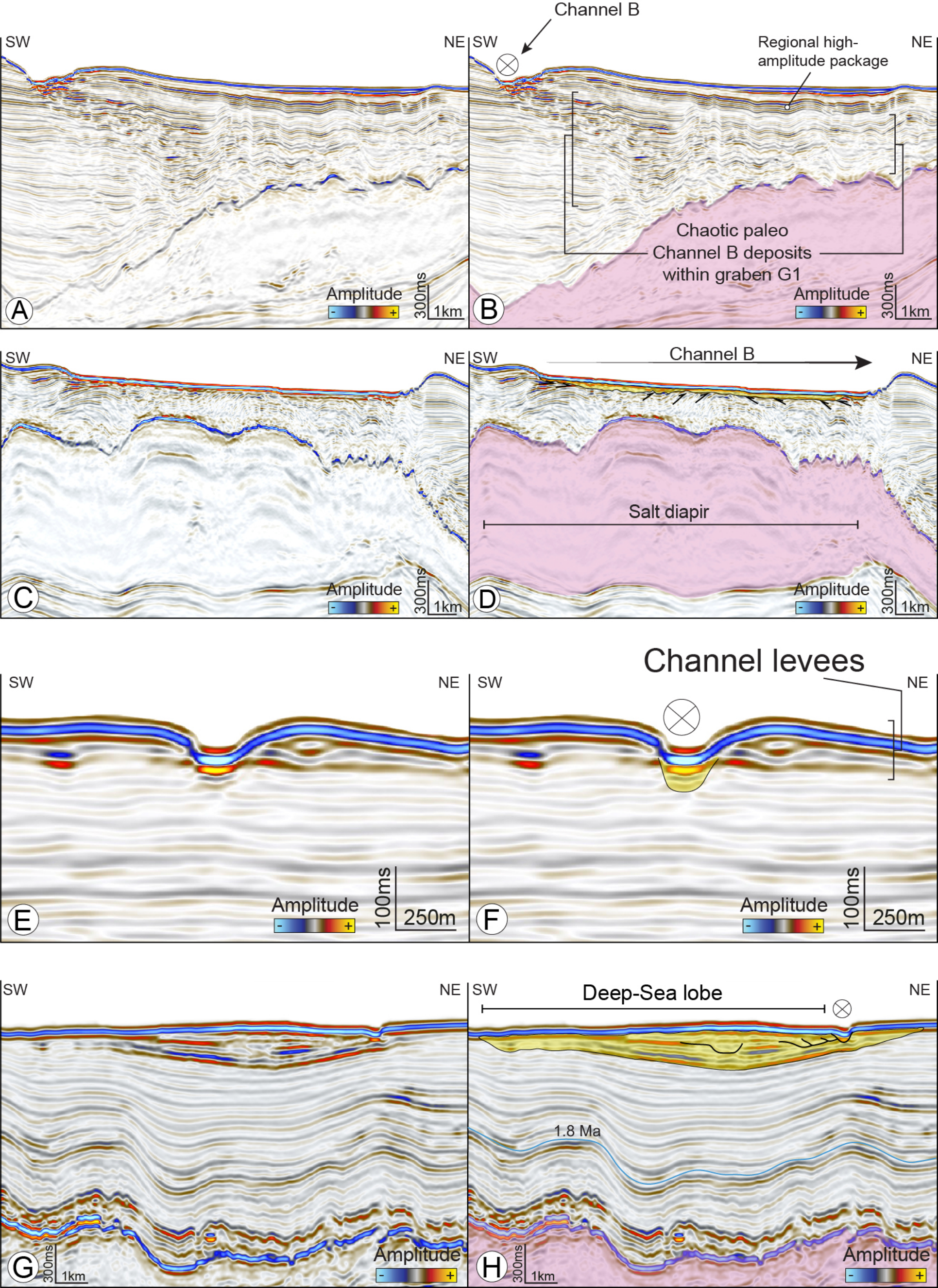

Channel B
SW
NE
SW
NE
Regional high-amplitude package
Chaotic paleo Channel B deposits within graben G1
Amplitude
300ms
1km
A
B
SW
NE
SW
Channel B
NE
Salt diapir
C
D
Channel levees
SW
NE
SW
NE
100ms
250m
E
F
SW
NE
SW
Deep-Sea lobe
NE
1.8 Ma
G
H